Desalination and Water Treatment
www.deswater.com
doi:10.5004/dwt.2021.27476

231 (2021) 113–130
August

Three-dimensional numerical analysis on a new design of hydraulic structure for water treatment

Wenrong Tu[a,*], Zhilin Sun[a], Shibiao Fang[b]

[a]*College of Civil Engineering and Architecture, Zhejiang University, Hangzhou 310058, China, Tel. +8619975273600; email: Twy8718@163.com (W. Tu), Tel. +8613606705667; email: 11812098@zju.edu.cn (Z. Sun), Tel. +8613757155013; email: wuyibiaobiao@163.com (S. Fang)*
[b]*Nanchang Institute of Technology, Nanchang 330044, China*

Received 23 November 2020; Accepted 30 May 2021

ABSTRACT

The bottom shaft driving flap gate is a new type of sluice gate, which is suitable for urban sewage water treatment. Although the bottom shaft driving flap gate has many advantages such as cheap investment and simple maintenance, it develops slowly because of the constraints of related technologies. As such, the flow pattern analysis and flow rate analysis on this hydraulic structure have important engineering significance. In this paper, a three-dimensional numerical simulation was used to analyze flow conditions of a new bottom shaft driving flap gate in the actual water control project. The CFX turbulence default model and non-slip grid technology were used to simulate the project under the same conditions of the test, and this research obtained the flow line, the flow rate of cloud images, and the velocity vectors of the model. Then this paper explained the reason for the flood conditions (once in 20 y, once in 50 y, once in 100 y) by analyzing the results. The research in this paper verifies the rationality of the model test and the effectiveness of the numerical simulation. The findings and conclusions of this paper provide the basis for the project implementation in a sediment-laden river and provide a reference for other similar projects.

Keywords: Bottom shaft driving flap gate; Three-dimensional numerical simulation; Turbulence model; Non-slip grid technology; Water treatment

1. Introduction

The bottom shaft driving flap gate is a new type of gate suitable for urban landscape water conservancy construction. At present, there is still no systematic research on the global. This type of gate will change the upstream and downstream plane flow field during the opening and closing process, affecting the upstream and downstream water levels of the gate. At the same time, the turbulent flow near the gate is very complicated. Under different operating conditions, the water flow pattern will be very different. Therefore, it is extremely important to study the flow pattern of the bottom gate drive flap gate experimentally and numerically.

The flow over hydraulic structures in open channels (such as sluice gates, dams, weirs, spillways) is very complicated. In the terms of nautical problems, bed and bank erosions and sediment transports [1], flow over spillways has been investigated by many researchers. Olsens and Kjellesvig [2] and Guo et al. [3] used numerical models to calculate the discharges through spillways. Song and Zhou [4] have coupled one-dimension and three-dimension models to simulate the flow over a spillway. Using the commercial CFD package Flow-3D, Savage and Johnson [5] have carried out numerical calculations for the flow over the spillway. Using the open-source CFD toolbox OpenFOAM, the study of dam-break flows has been carried out by Biscarini et al. [6]. Nguyen and Nestman [7] have used two commercial

* Corresponding author.

1944-3994/1944-3986 © 2021 Desalination Publications. All rights reserved.

CFD software packages, FIDAP and Comet, to calculate the turbulent flows over hydraulic structures in natural rivers, however, FIDAP and Comet are not well designed for river flows. In the terms of the numerical errors associated with the discretization of the equations on the grid [8], setting up inlet boundary conditions for LES (large eddy simulation) is a very significant key method, which can strongly affect simulation quality. There are some alternatives to deal with LES suggested by Lund et al. [9], Klein et al. [10], Ferrante and Elgobashi [11], etc. Furthermore, the validation of the results from LES is somehow impossible due to limitation of observation data from field surveys.

With the continuous expansion of urban scale and the continuous increase of sewage discharge, hydraulic structure facility plays an increasingly important role in wastewater treatment and water reuse. Urban sewage treatment facilities mainly include wastewater discharge channel, water retaining structure (such as sluice gate), flocculation and sedimentation tank, and water treatment plant. Sediment retention is an important process in water treatment technology, and its effect is directly related to the water purification effect and economic cost. In flocculation and sedimentation, the water flow speed is required to be slow to ensure the stable sedimentation of flocs. Therefore, we need to equip a hydraulic flap gate in front of the flocculation tank and sedimentation tank to ensure a smooth flow, removing a portion of sediment. In this way, we can improve the flocculation and sedimentation effect. However, in the actual operation, it is difficult to guarantee the effect of the flap gate, and it is difficult to measure the velocity distribution of the channel at the gate completely and carefully. The computational fluid dynamics method can solve this problem well. In this paper, the Fluent software is used to establish the flow channel model at the sluice gate for numerical simulation, and the detailed velocity distribution data can be obtained, which is of great significance to optimize the sewage treatment facilities and improve the flocculation and sedimentation effect. Therefore, in this research, we apply the Finite Volume Method combined with the RANS approach (two-equation k-ε model) to simulate free-surface flows over hydraulic structures with flap gate. Numerical results are validated against typical benchmarking experiments in Yangzhou University, and field survey data is from the Water Affairs Bureau of Sucheng District, Suqian City, at Jiangsu Province. Some parameters (turbulence characteristics, three-dimensional free surface profile, etc.) have been obtained from the laboratory, and we try to compare our numerical results with the experiment's results.

2. Materials and methods

According to the similarity criterion of the hydraulic model, the physical model of the bottom shaft driving flap gate was established and the suitable methods and equipment for testing the physical model were selected. During the experiment, the corresponding values of the flow velocities of 13 mainstream sections were recorded. Flow patterns of the surface water layer were observed through plastic suspended particles, and the bottom flow patterns were displayed by a chemical tracer.

2.1. Experimental setup

In the physical model experiment, the water flow must be similar to the actual flow, thus the gravity similarity criterion is adopted to ensure that all kinds of hydraulic phenomena are similar. The gravity similarity criterion according to the Froude criterion is shown below.

$$F_r = \frac{v_r}{\sqrt{g_r l_r}} = 1 \tag{1}$$

Based on the actual project size and layout, a maximum model scale is selected in Testing Hall to enhance the reliability of the physical model experiment. The model geometric scale was 1:20, and other hydraulic characteristics are shown in the following.

Geometric scale: $\lambda_r = l_p/l_m = 20.000$
Velocity ratio: $v_r = \lambda_r^{1/2} = 4.472$
Time scale: $T_r = \lambda_r^{1/2} = 4.472$
Discharge scale: $Q_r = \lambda_r^{5/2} = 1{,}788.854$
Roughness scale: $n_r = \lambda_r^{1/6} = 1.648$
l: length.
r: rate of the practical value to model value.
p: practical value.
m: model value.

According to the geometric scale of 1:20, the overall model length is about 15.675 m. The upstream river width is 5.500 m, with a length of 8.500 m. The downstream river width is 5.000 m, with a length of 4.000 m. The upstream connected segment is 1.000 m, and the downstream connected segment is 1.643 m. The length of the gate chamber segment is 0.540 m, with a net width of 0.900 m. The roughness of the prototype is n_p = 0.011~0.020, and it is made of reinforced concrete. As such, the roughness of the physical model is n_m = 0.011~0.020/1.648 = 0.007~0.012. In accordance with this range, the calcareous plates (n_m = 0.007~0.010) are used to make a physical model, the gate is made of stainless steel. The hydraulic model is shown in Fig. 1.

2.2. Numerical calculation method

The basic method of discretization is the method of how to convert derivatives (or integrals) controlling the equation into discrete numerical values. The discretization of

Fig. 1. Overall layout of the physical model.

partial differential equations is called the finite difference method, and the discretization of integral form equations is called the finite volume method. CFX uses finite elements to acquire the numerical accuracy of the finite element method on the basis of the conservative properties of FVM.

FVM is considered as a kind of numerical solving method between FDM and FEM [12], which is also known as the control volume method (CVM). FVM is a form of important numerical solving method separated from the original FDM, along with the continuous improvement of the calculation method. The corresponding basic idea is that the calculation region is divided into grids, making the surrounding of each mesh have a non-duplicated control volume; the partial differential equation to be solved is for the integration of each control volume; thus, a set of discrete equations can be obtained in which the unknown quantity is the feature variable at the grid points.

The FVM departure equation is the fluid motion equation (continuity equation, momentum equation, and turbulent model k-ε equation), integrating each control volume for the conservative form of the control equation to obtain a discrete control equation:

$$\frac{\partial}{\partial t}\left(\int_{\Delta V}\rho\varphi dV\right)+\int_{A}n\left(\rho u\varphi\right)dA=\int_{A}n\left(\Gamma\cdot\mathrm{grad}\varphi\right)dA+\int_{\Delta V}SdV \tag{2}$$

where the physical meaning of each term is as follows: the first term on the left equation represents the amount of change of the characteristic variable φ within the control volume over time, and second term on the left represents the net increase amount of the characteristic variable φ caused by boundary diffusion in the control volume, the first term on the right equation represents the net increase amount of the characteristic variable φ caused by boundary diffusion in the control volume, and the second term on the right represents the amount produced by the internal source of the characteristic variable φ within the control volume.

The conservative relationship of the characteristic variable φ within the control volume can be expressed as follows:

$$\varphi_{\text{change with time}}+\varphi_{\text{net reduction caused by boundary convection}}=\varphi_{\text{net increase in boundary diffusion}}+\varphi_{\text{amount produced by the inner source}} \tag{3}$$

In the steady-state, since the time-dependent term is equal to zero, Eq. (13) can be written as:

$$\int_{A}n\left(\rho u\varphi\right)dA=\int_{A}n\left(\Gamma\cdot\mathrm{grad}\varphi\right)dA+\int_{\Delta V}SdV \tag{4}$$

The volume fraction reduces the equation order, and the requirements for calculating the grids are also reduced. This is an outstanding advantage of FVM. When using FVM, the mesh is used to divide the computational domain into a number of small finite control volumes (CVs), different from the difference method, FVM definition is the surface of limited volume (a side in 2D), rather than the node. Normally, we use the appropriate grid to define the control volume, selecting the computational point in the center of the control volume.

2.3. Free surface treatment

The free surface issue has been a very important research subject in computational fluid dynamics (CFD), where the rationality of free surface simulation is directly related to the reliability and accuracy of numerical simulation results. The main methods used for free surface simulation are generally the rigid-lid hypothesis, height function (HOF) [13], marker and cell (MAC) [14–15], volume ratio function (VOF) [16], level set [17], and other methods. Since the simulation in this paper is about the flat free surface water-flow problem of a large area, the rigid-lid hypothesis method is adopted for the simulation. The rigid-lid hypothesis assumes the free liquid surface is a fixed regular and movable wall, directly using the 'non-penetrating' condition of the fixed wall, the value of each variable in the normal direction is zero, and the gradient value in the tangential direction is zero. The rigid-lid hypothesis is simple and easy to understand, and it is relatively simple in processing the numerical computation.

For introducing the mathematical model adopted for the numerical simulation of the shaft bottom flap gate in this paper, the corresponding control equations, including the continuity equation and the equation for conservation of momentum, are explained. The standard k-ε model is selected for the turbulence model, and finite volume method is adopted as the numerical computation method to conduct the processing of the rigid-lid hypothesis of the free surface, and the SIMPLE series algorithms (SIM2PLEC) are used to solve pressure-velocity coupling.

3. Numerical simulation of a hydraulic structure in open channels with a water-retaining gate

There is a new type of bottom shaft driving flap gate in the real world pending construction, which will be located in the Ancient Yellow River. Therefore, this project is taken as the case study in this paper in order to analyze the distribution of flow velocity and hydraulic design rationality of the new bottom shaft driving flap gate. Also, the flow velocity measurement and forecast under different discharges and water levels near the gate are required to determine the best operation mode of the gate. The overall length of this water control project is about 313.500 m. The upstream river width is 110.000 m, with a length of 170.000 m. The downstream river width is 100.000 m, with a length of 80.000 m. The upstream connected segment is 19.840 m, and the downstream connected segment is 32.860 m. The length of the gate chamber segment is 10.800 m, with a net width of 18.000 m. There is an overflow dam located on each side of the gate chamber, with a horizontal range of 20.000 m, respectively.

3.1. Three-dimensional numerical model of the bottom shaft driving flap gate

3.1.1. Introduction of the model

This paper adopts computational fluid dynamics software ANSYS CFX to build the computational domain, and the geometry size of the numerical model is the same as the prototype in practice. ANSYS CFX is a high-performance computational fluid dynamics (CFD) software tool

that delivers reliable and accurate solutions quickly and robustly across a wide range of CFD and multi-physics applications. The manufacturer and software company of CFX is ANSYS, Inc., located in the USA. The professional mapping software of AutoCAD (Autodesk Computer-Aided Design) has been used to complete the geometric modeling in this paper, which is imported into the ANSYS ICEM CFD preprocessor of ANSYS CFX. The grid dividing of the model is conducted through the use of the powerful grid dividing function of ANSYS ICEM CFD and a tetrahedral structural mesh type. In order to improve the mesh quality, it is densified in the vicinity of the gate. After meshing, the appropriate boundary condition is given in ANSYS ICEM CFD, which lays the foundation for setting the boundary condition when conducting the subsequent CFD simulation.

3.1.2. Geometry modeling

The water flow pattern of the bottom shaft driving flap gate is under the flood conditions of once in every 20 y, once in every 50 y and once in every 100 y. First, we use AutoCAD to establish the 3D model of the solid structural part, and then we create three geometric fluid models, respectively, according to the different upstream and downstream water levels of these conditions. The solid part of the designed 3D numerical model of the hydro project is shown in Fig. 2.

3.1.3. Overall mesh distribution

The tetrahedral grid units are used for the computational grid throughout the computational domain. Since the analog river section is relatively large and the geometry is a completely symmetrical structure, the simulation uses half of the model structure in order to accelerate the convergence rate of the numerical calculation. Thus, more grids can be arranged in the vicinity of the gate, and the simulation will better display the hydrodynamic phenomena near the gate as shown in Fig. 3.

3.1.4. Gate mesh distribution

In this paper, the gate itself, and near the bottom, piers, and overflow dam, are densified. Since the water flow change at the gate is more intense, the flow phenomenon is also more complex. The boundary layer separation phenomenon near the gate is especially easy to increase the shape resistance of the gate. Therefore, the focused refinement is conducted for the boundary grid near the gate segment as shown in Figs. 4 and 5.

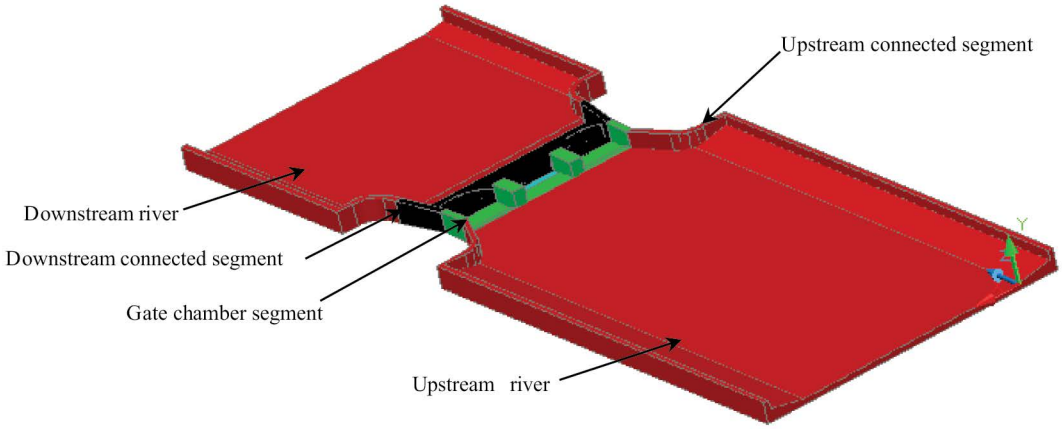

Fig. 2. 3D numerical simulation model.

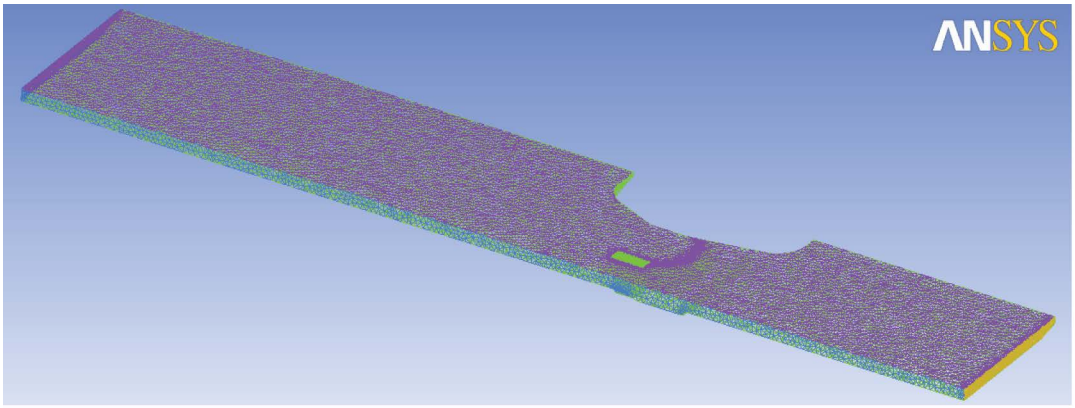

Fig. 3. Model's computing domain grid arrangement schematic diagram.

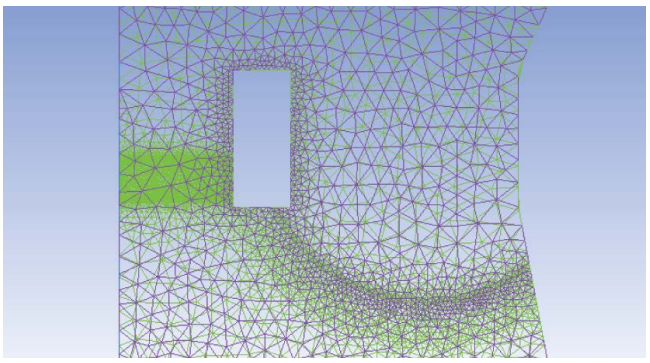

Fig. 4. Local surface mesh refinement.

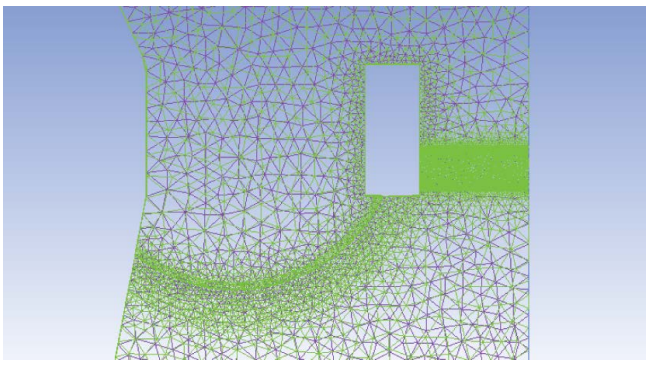

Fig. 5. Local bottom mesh refinement.

3.2. Model boundary conditions

3.2.1. Wall treatment

The flow pattern of the fluid at the wall is divided into two types: non-slip and freedom slip. In this paper, we set it as the non-slip wall condition by using the given automatic wall functions in CFX. The main idea is to adjust the ω value between the logarithmic equation and nearby wall, so that it can automatically adjust the equation according to the location to meet the wall conditions. The *k* equation flux is manually specified as zero, the momentum equation is derived from the velocity, via the corresponding equation:

$$F_U = -\rho u_\tau u^* \tag{5}$$

where:

$$u_\tau = \sqrt{v\left|\frac{\Delta U}{\Delta y}\right|} \tag{6}$$

$$u^* = \max\left(\sqrt{a_1 k}, u_\tau\right) \tag{7}$$

The ω formula specifies the algebraic expression; its equation is:

$$\omega_1 = \frac{u^*}{a_1 k y} = \frac{1}{a_1 k v}\frac{u^{*2}}{y^+} \tag{8}$$

The corresponding sub-layer expression is:

$$\omega_s = \frac{6v}{\beta(\Delta y)^2} \tag{9}$$

where Δy is the distance between two grid nodes nearest to the wall. In order to avoid the cycle convergence behavior, we use the following equation:

$$\omega_\omega = \omega_s\sqrt{1+\left(\frac{\omega_1}{\omega_s}\right)^2} \tag{10}$$

3.2.2. Boundary condition setting

In this model, the upstream runoff section is taken as the boundary condition of the velocity inlet, and the downstream river outlet is taken as the boundary condition of the velocity outlet, given that the boundary velocity of the upstream segment and downstream segment water level varies with a change in time. Since the rigid-lid hypothesis method is used for the free surface, the choice of the symmetry boundary condition is used on the surface, namely, the normal velocity of wall fluid $u_n = 0$. The non-slip wall boundary condition is selected for the remaining boundaries, namely, the normal velocity and tangential velocity of the wall fluid is zero, $u_i = 0$ (i = 1,2,3). Fig. 6 shows the model boundary setting schematic diagram.

3.3. Inlet conditions for turbulence and velocity

Table 1 is the conditions of prototype in practice, and is the inlet conditions of velocity and water depth for numerical simulation. And the inlet flow is established at the upstream gate.

3.4. Simulation results and analysis

3.4.1. Streamline

The numerical simulation includes the flood conditions of once every 20 y, once every 50 y, and once every 100 y. Through the calculation of ANSYS CFX-POST CFD software, the flow lines of the three conditions are obtained, as shown in Figs. 7–9.

It can be seen from the figures that the water flow under the flood condition of once every 20 y is relatively gentle, and the whirlpool mainly occurs in the downstream central location. The flow line chart of flood condition occurring once every 50 y is very similar to the flow line chart of flood conditions occurring once every 100 y, and the water flow is not so gentle. This is because the water flows through the overflow dam forming a water level difference, causing the downstream water level to be relatively disordered. The formed whirlpool region is more deviated from the direction of the wall side in Figs. 8 and 9.

3.4.2. Flow velocity

Figs. 10–15 are the flow velocity cloud pictures and flow velocity vector diagrams under the three flood conditions of

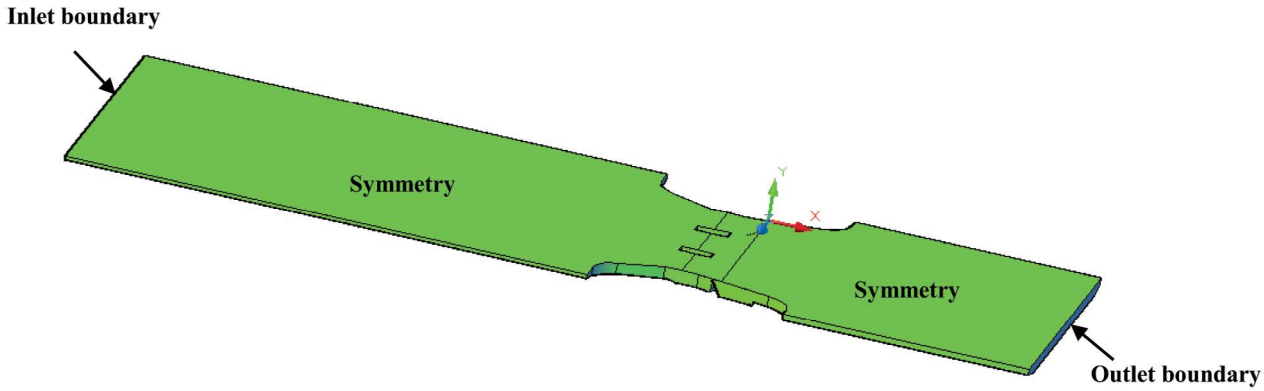

Fig. 6. Schematic diagram of model boundary condition.

Table 1
Inlet conditions analysis table (according to prototype size)

Conditions		Discharge (m^3/s)	Water depth of upstream gate (m)	Water depth of downstream gate (m)
Condition 1	Once in 20 y	87.000	3.000	2.870
Condition 2	Once in 50 y	101.000	3.088	2.928
Condition 3	Once in 100 y	111.000	3.200	3.010

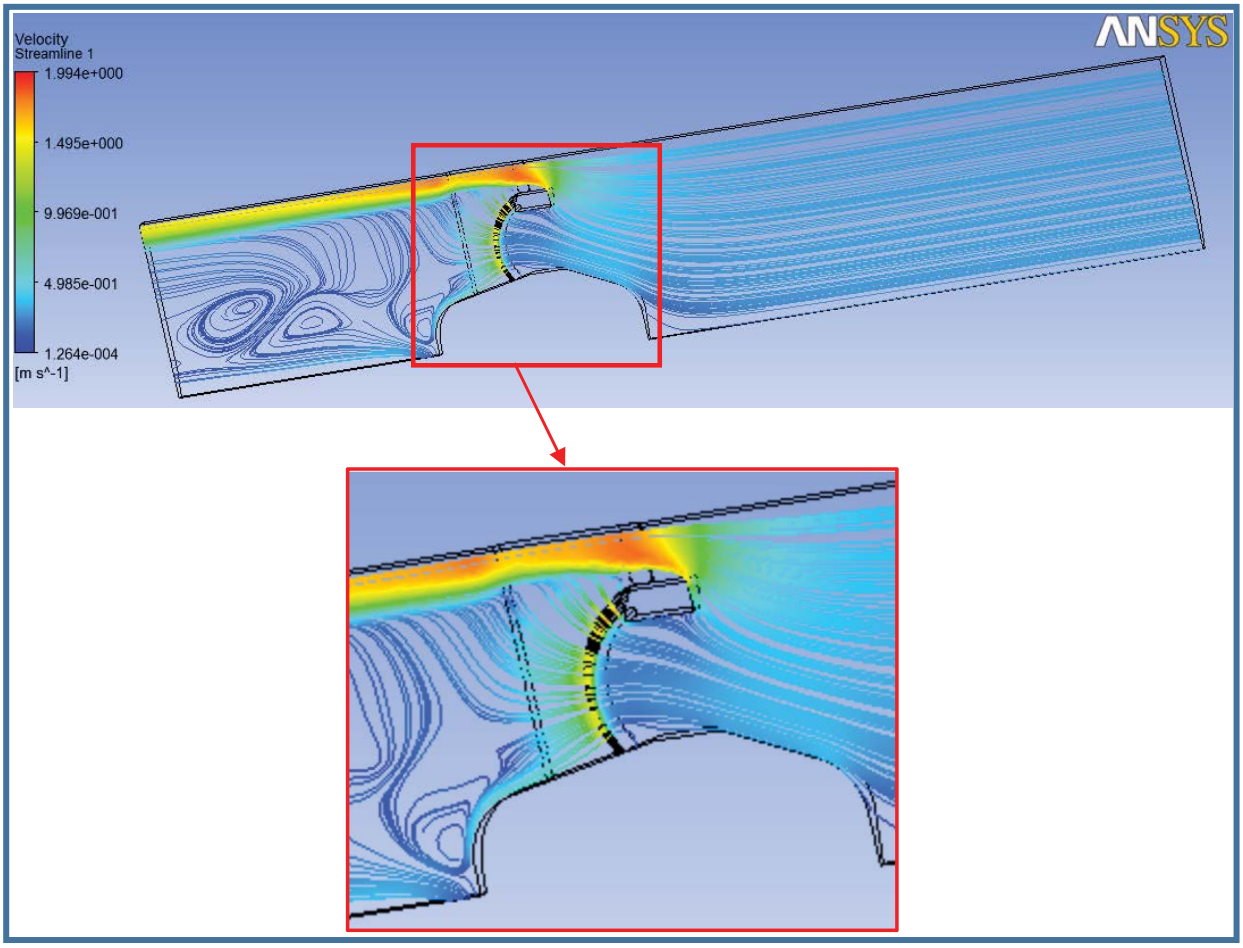

Fig. 7. Surface layer streamline chart under the flood condition of once every 20 y.

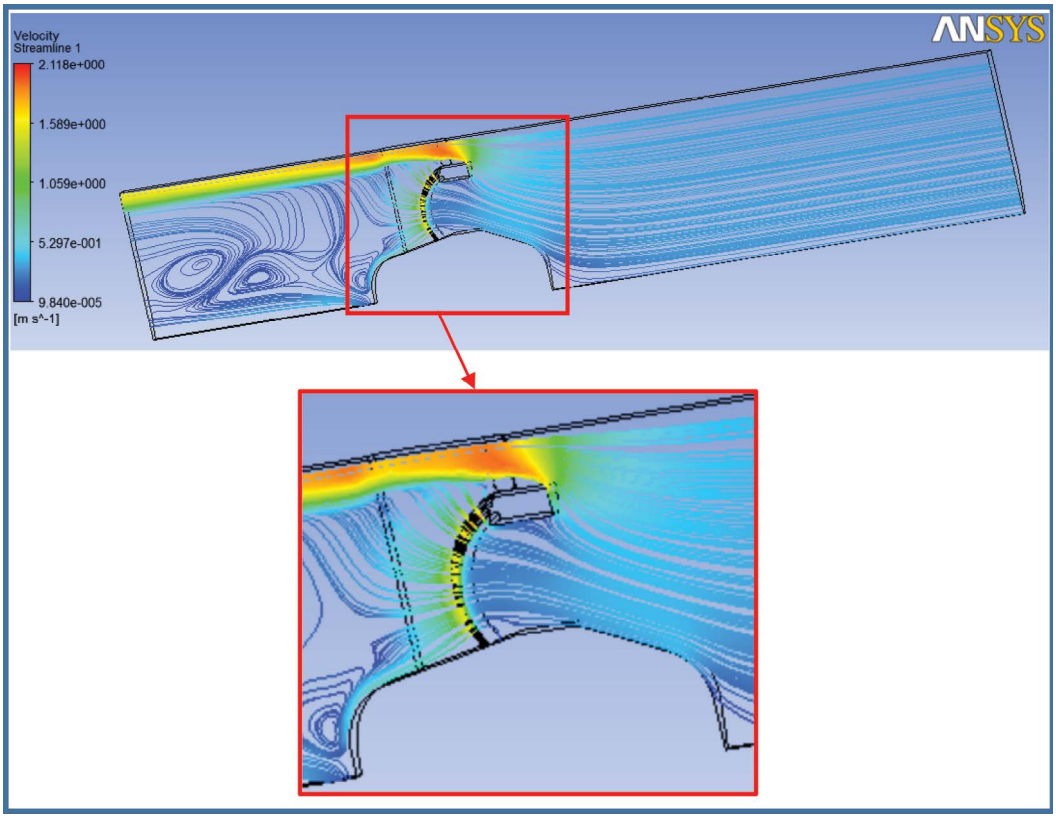

Fig. 8. Surface layer streamline chart under the flood condition of once every 50 y.

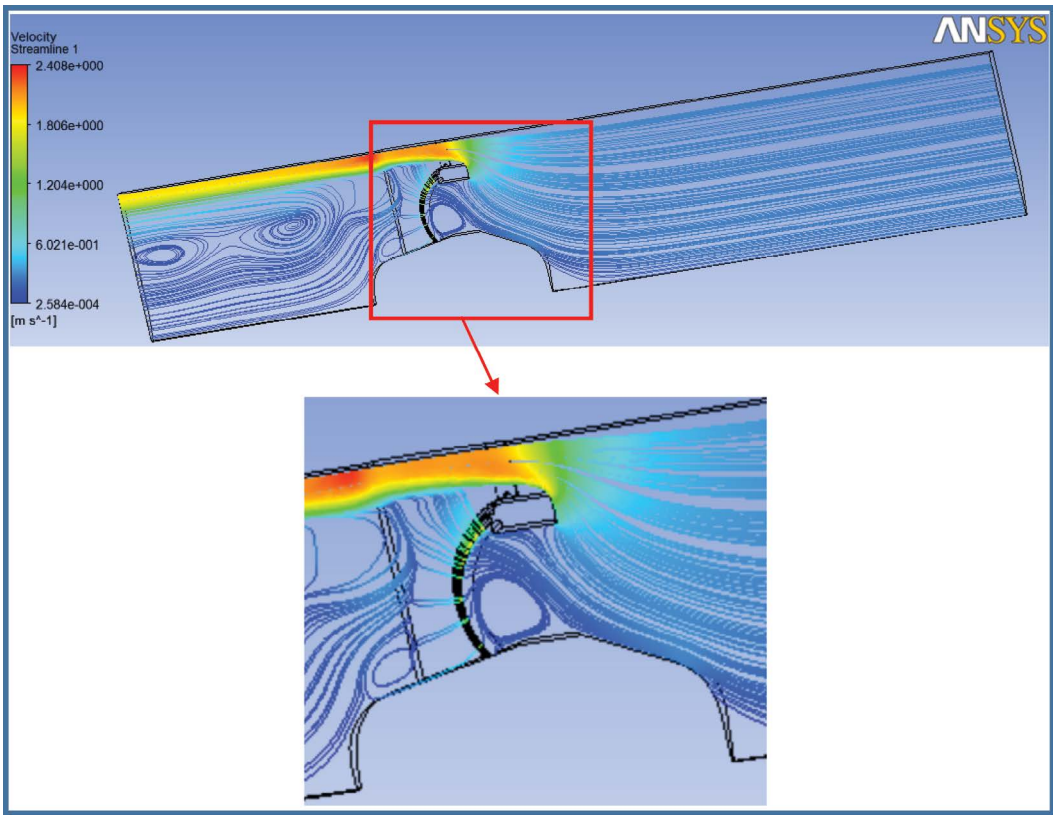

Fig. 9. Surface layer streamline chart under the flood condition of once every 100 y.

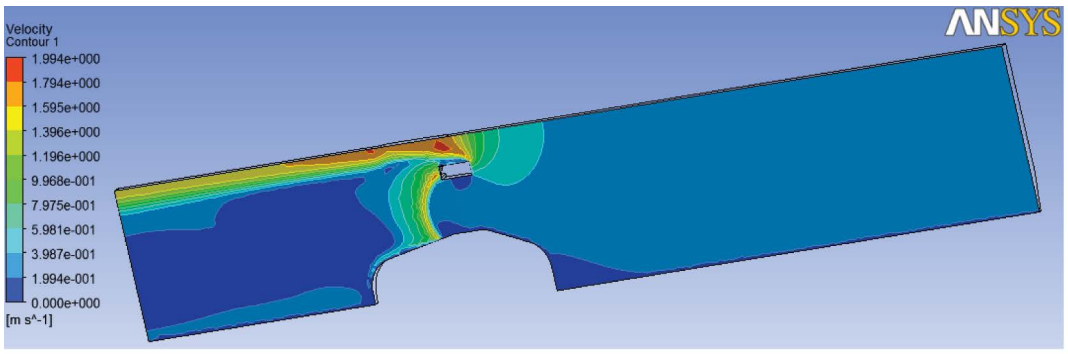

Fig. 10. Flow velocity distribution cloud chart under the flood condition of once every 20 y.

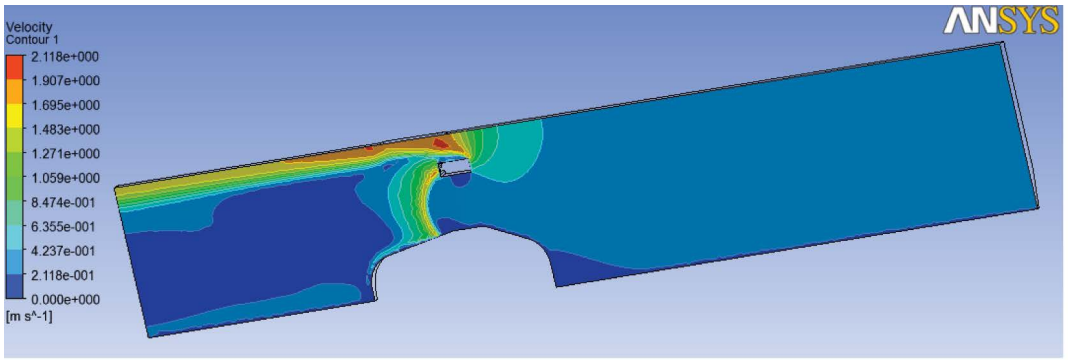

Fig. 11. Flow velocity distribution cloud chart under the flood condition of once every 50 y.

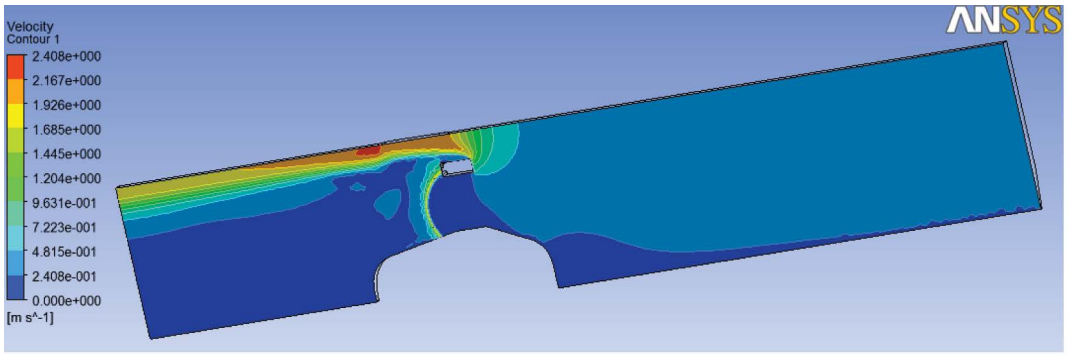

Fig. 12. Flow velocity distribution cloud chart under the flood condition of once every 100 y.

once every 20 y, once every 50 y, and once every 100 y. It can be seen that the flow velocity cloud pictures of the three flood conditions are generally more consistent with each other: the largest flow velocity mainly occurs in the vicinity of the reduction segment of the pier section, and the flow velocity of the water flow in the middle portion of the river has stretched through reduction of the section. The following are the flow velocity distribution cloud diagrams and flow velocity vector diagrams under various flood conditions:

According to the figures above, the impact scope of the gate pier on the flow velocity increases along with the increase of water level, and the impact scopes of the flood conditions of once every 50 y and once every 100 y are significantly greater than the flood condition of once every 20 y. There is an almost still water region in the connecting portion of upstream slope protection and arc segments with an extremely small flow velocity, and the scope of the small flow velocity region under the flood condition of once every 20 y is relatively large.

4. Results

After the processing is conducted by using the CFX-POST software, the numerical simulation data is connected to the model measuring points, outputting velocity vector data on each measurement line. As shown in Fig. 16, the measurement line location is consistent with the line location of the experimental measuring points.

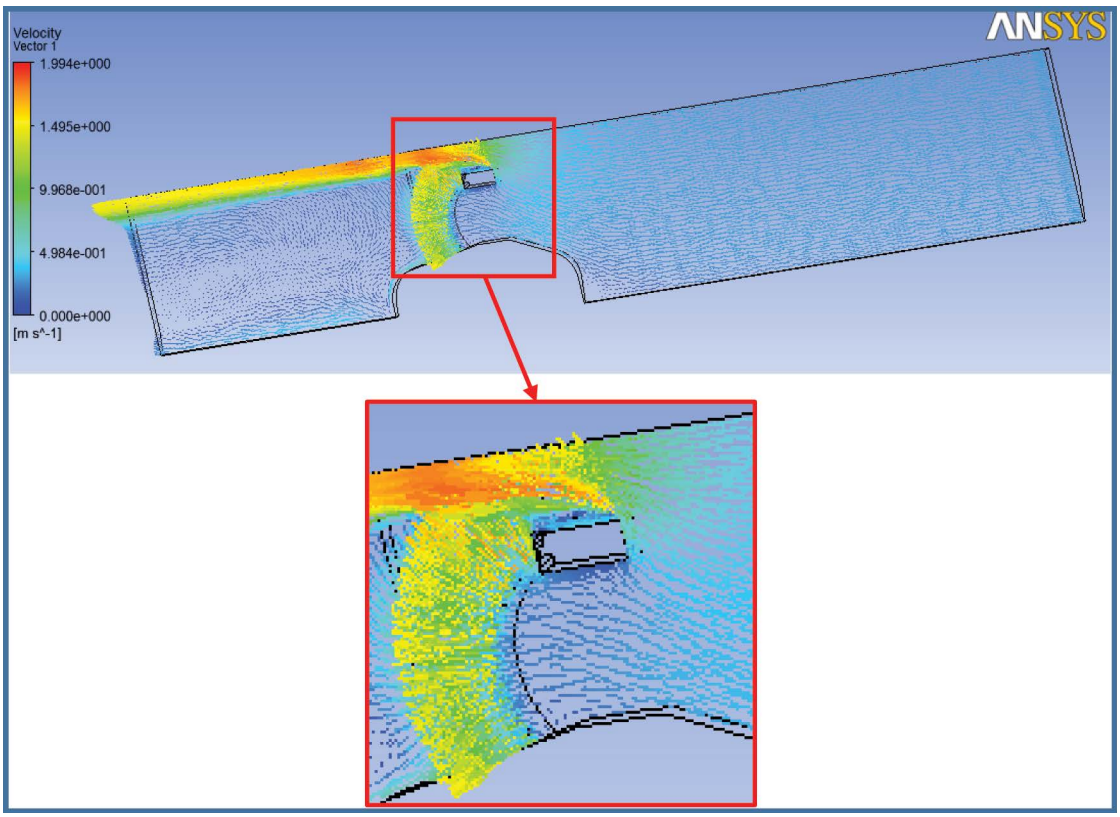

Fig. 13. Velocity vector chart under the flood condition of once every 20 y.

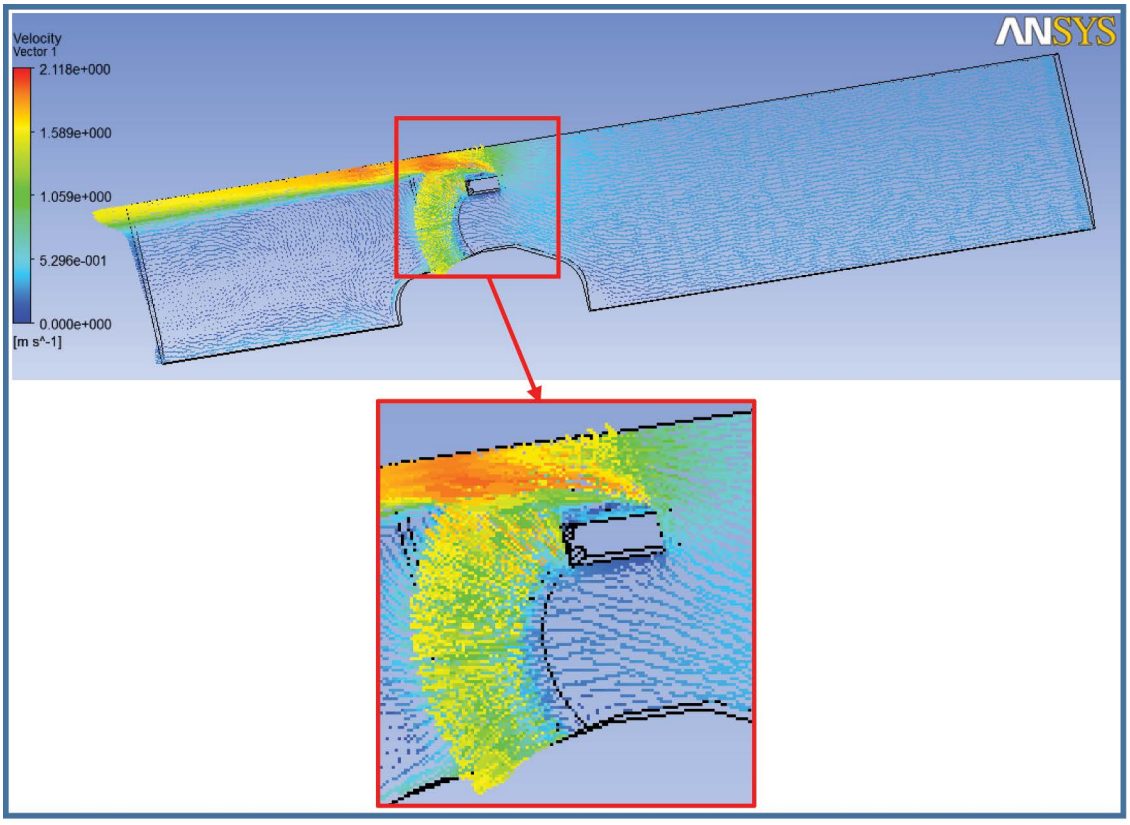

Fig. 14. Velocity vector chart under the flood condition of once every 50 y.

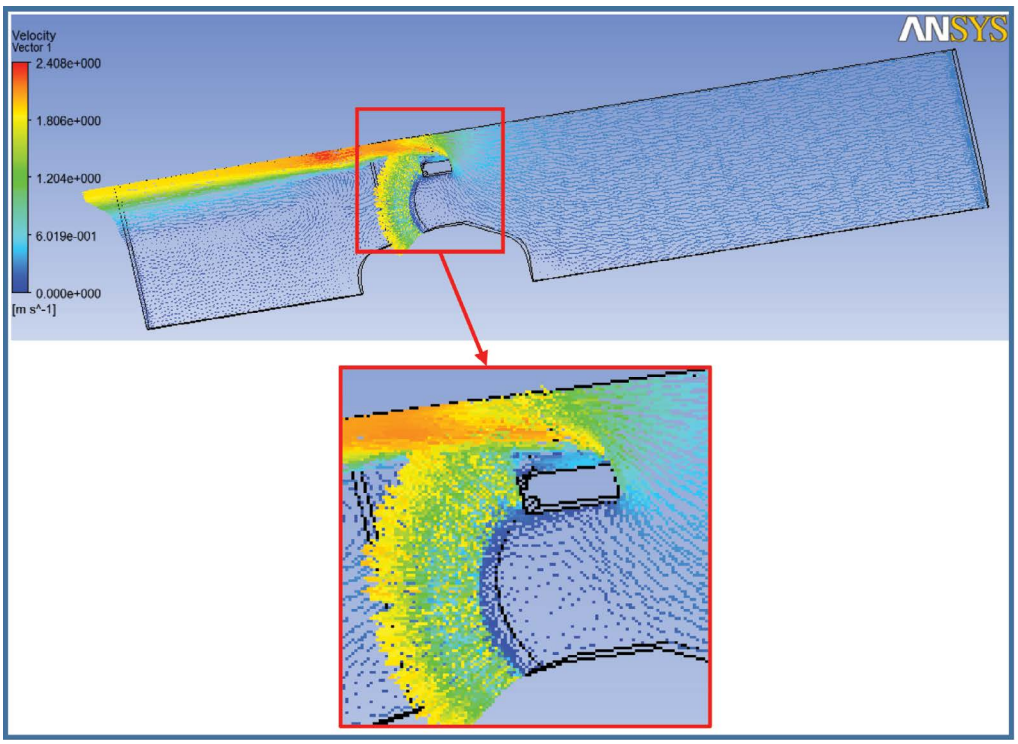

Fig. 15. Velocity vector chart under the flood condition of once every 100 y.

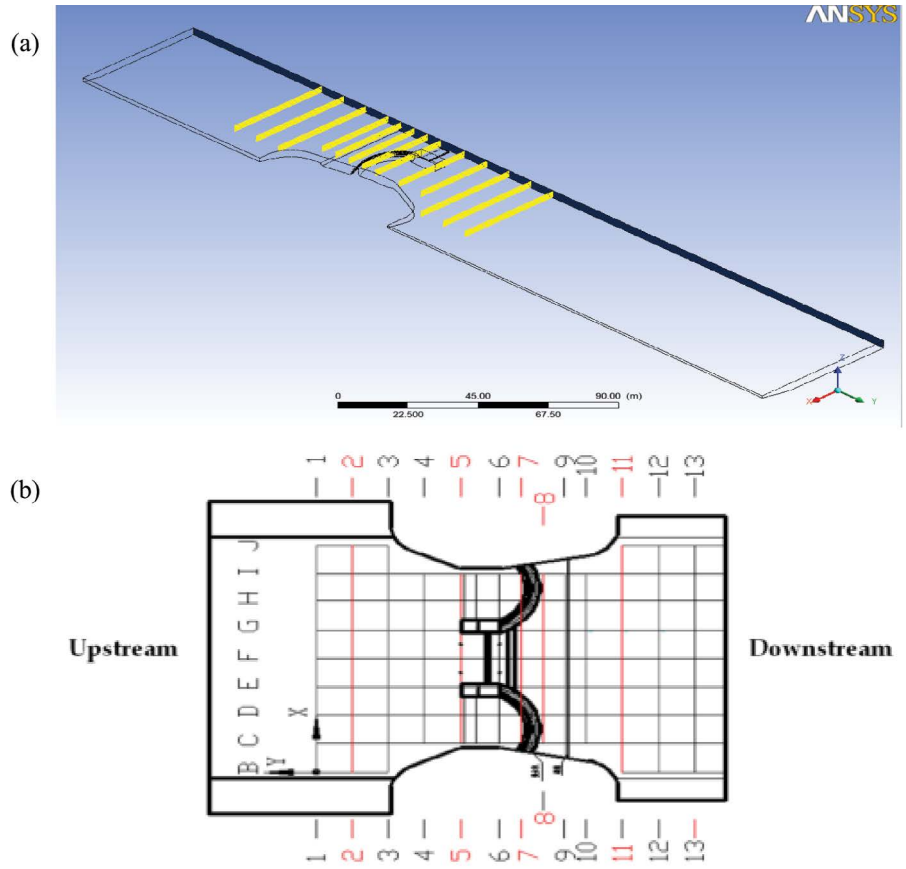

Fig. 16. (a) Velocity measurement line schematic diagram and (b) test sectional distribution chart.

We select the middle sections 2-2, 5-5, 7-7, 8-8, and 11-11 of the flood condition occurring once every 50 y as the representative for drawing flow velocity distribution curves.

It can be seen from Fig. 17 that the flow velocity distribution on the 2-2 section is more regular, together with a more uniform velocity and a smaller range of changes. The velocity decreases on both sides by starting from the model's middle line, essentially showing a linear relationship, and velocity decreases from the topmost to the bottom along the direction of depth.

Fig. 18 is the relation curve between the 5-5 sectional velocity and the perpendicular flow direction under the flood condition of once every 50 y. It can be seen that the velocities are small on both sides, and the velocity in the middle part is very large. The velocity at the model midline obtained by numerical simulation is smaller than the velocity in the actual location near the gate pier.

It can be seen in Fig. 19 that there is a dramatic velocity change along the *x*-direction in the 7-7 section located at a distance of 3.088 m from the bottom in comparison with other water depths (0.618 m, 1.236 m, 1.854 m and 2.470 m), and the velocities on both sides of the other layers are smaller. Through the analysis, the reason for flow velocity changes of the topmost measuring points is that the sectional water level is much higher than the overflow dam, forming a larger water level drop to form a large flow velocity.

In Fig. 20, the 8-8 sectional flow velocity distribution change is more dramatic compared to the 7-7 sectional flow velocity. This is mainly because the 8-8 cross-section is downstream of the overflow dam. After that, the upper

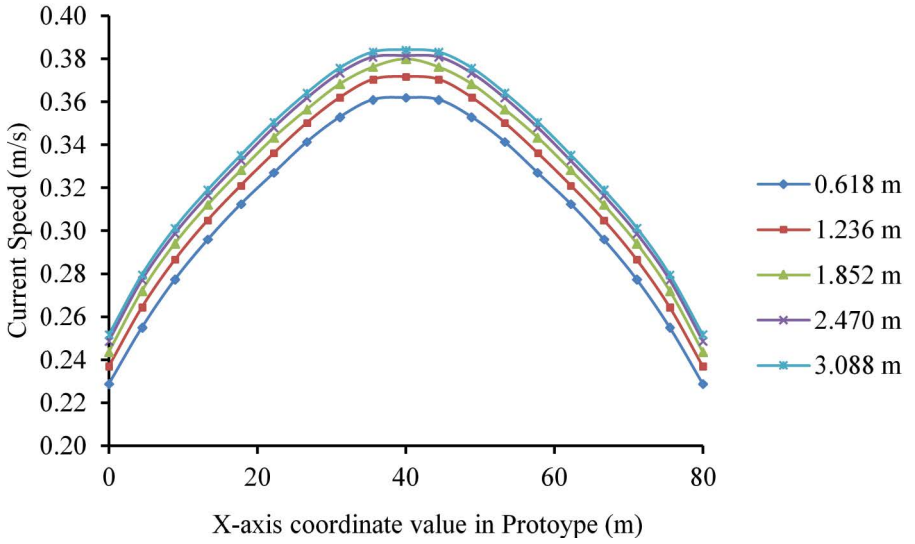

Fig. 17. Relation curve between the 2-2 sectional velocity and the perpendicular flow direction under the flood condition of once every 50 y.

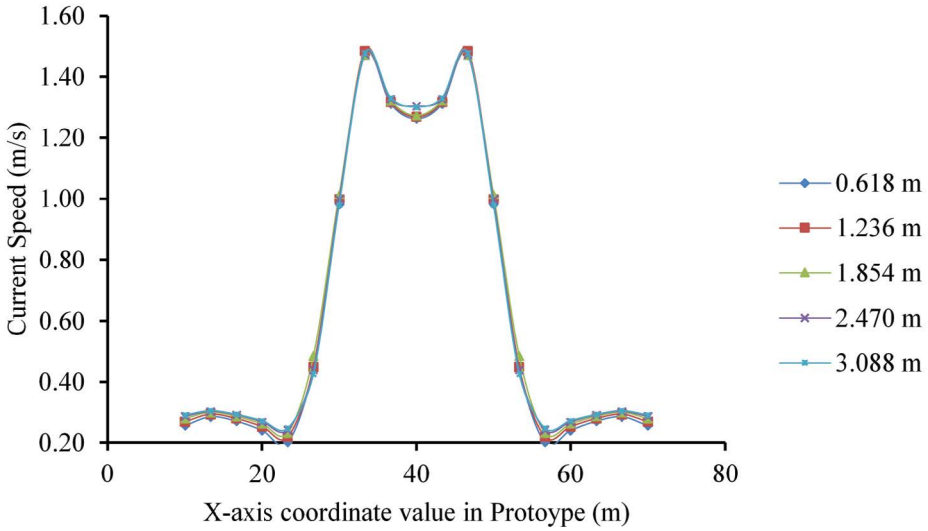

Fig. 18. Relation curve between the 5-5 sectional velocity and the perpendicular flow direction under the flood condition of once every 50 y.

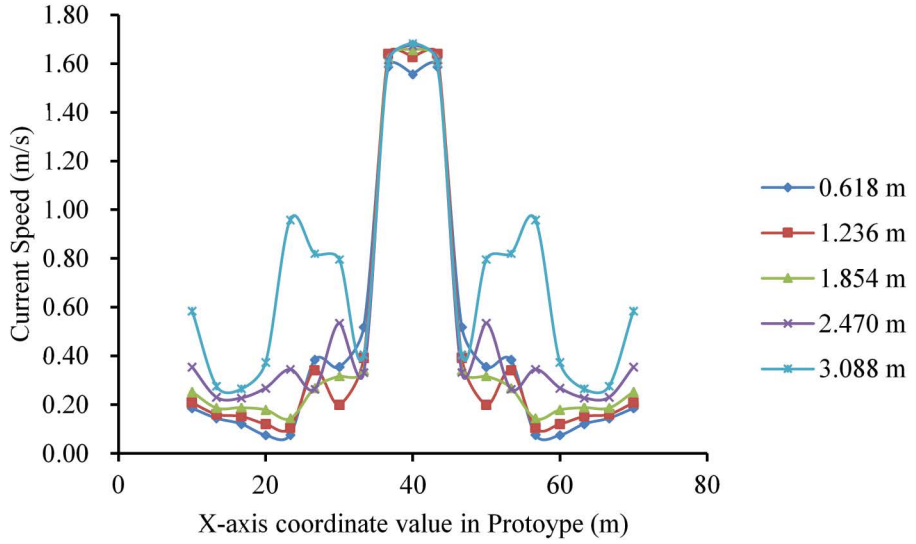

Fig. 19. Relation curve between the 7-7 sectional velocity and the perpendicular flow direction under the flood condition of once every 50 y.

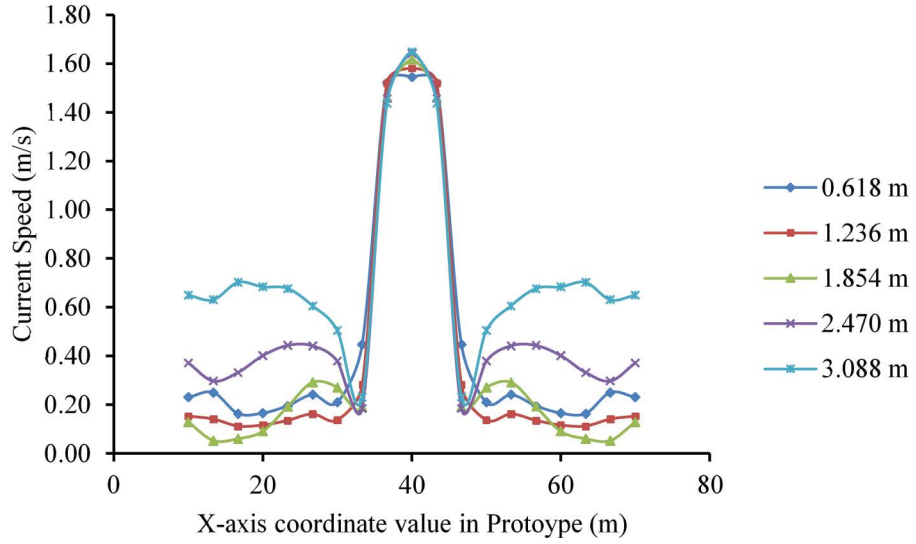

Fig. 20. Relation curve between the 8-8 sectional velocity and the perpendicular flow direction under the flood condition of once every 50 y.

part of the water level forms a drop. There is a relatively large water flow passing through the 8-8 cross-section, and there is a steep slope at the front end of the base plate which, to a certain degree, increases the flow velocity of the cross-section. As such, there is a dramatic change in the flow velocity under the combined effect of the large water flow and steep slope. However, the above two cross-sections are still of the situation that the central flow velocity is much greater than the flow velocity on both sides.

It can be seen from the 11-11 sectional flow velocity distribution curve in Fig. 21 that there is a larger flow velocity change near the bottom layer of the downstream segment, and the flow velocity on both sides of the model decreases with the increasing water depth of the measuring point. This is mainly due to the impact of the steep slope at the base plate. However, the flow velocity of the midline of the model increases with the increase of the water level. The flow velocity of the cross-section is more complex, which is mainly due to the impact of the formation of the vortex at the top surface.

5. Discussion

The flow velocity obtained respectively from the model experiment and numerical calculation is drawn into a curve diagram. Considering there are too many measuring layers at each section in the model experiment, we select the measuring points of the topmost layer, second layer and lowermost layer to validate the numerical simulation results. Section 2-2, section 5-5 nearby the gate pier, section 7-7,

section 8-8 and section 11-11 are selected as typical cross-sections under the flood condition of once in 50 y.

It can be seen that there is some difference between the data obtained from the experiment and results obtained from numerical simulation, but the overall trend is consistent in Fig. 22. The flow velocity obtained from the model experiment has more dramatic changes along with the *x*-axis. Flow velocity distribution obtained from the numerical simulation is smoothly transited from the centerline to both sides. Through the analysis, the main reason is that numerical simulation is in the hydrostatic state, while the experiment is in a dynamic water state. That is because the pumping force in the hydraulic experiment has an influence on the stability of water flow.

Fig. 23 is the comparative chart of 5-5 sectional velocity of numerical simulation with experimental results under flood conditions of once in 50 y. It can be seen from Fig. 23 that there is a good agreement between numerical simulation results and experimental data except for some individual points. In Fig. 24, there is a good agreement between numerical simulation results with experimental data, but the flow velocity of the topmost layer obtained by numerical

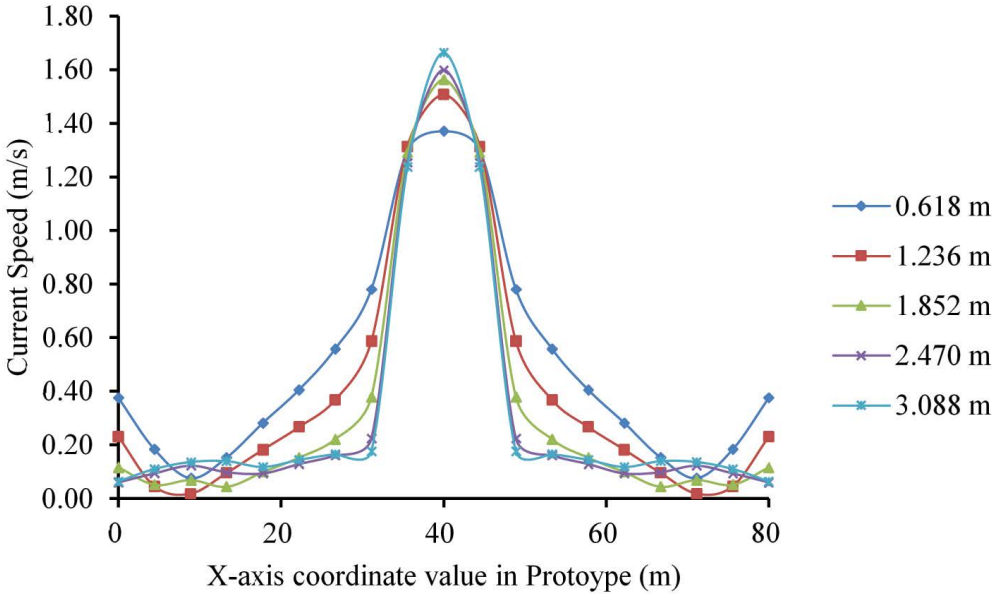

Fig. 21. Relation curve between the 11-11 sectional velocity and the perpendicular flow direction under the flood condition of once every 50 y.

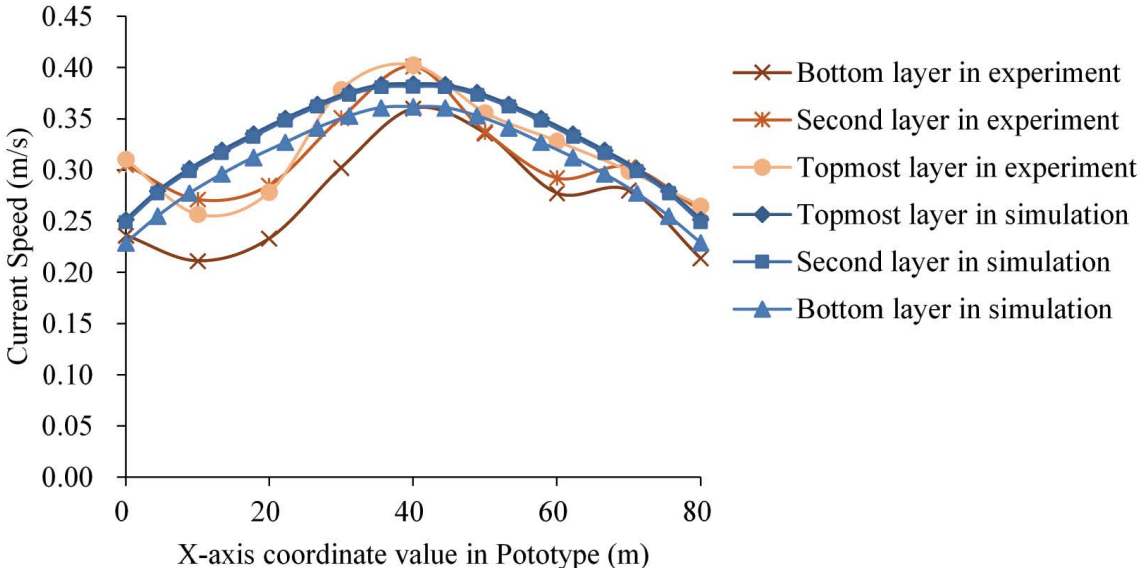

Fig. 22. Comparative chart of 2-2 sectional velocity of numerical simulation with experimental results under flood condition of once in 50 y.

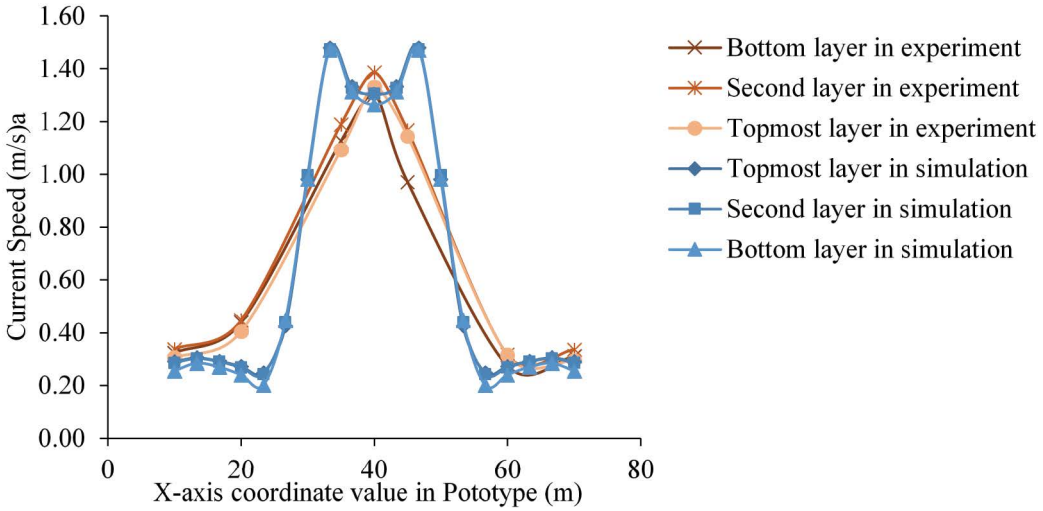

Fig. 23. Comparative chart of 5-5 sectional velocity of numerical simulation with experimental results under flood condition of once in 50 y.

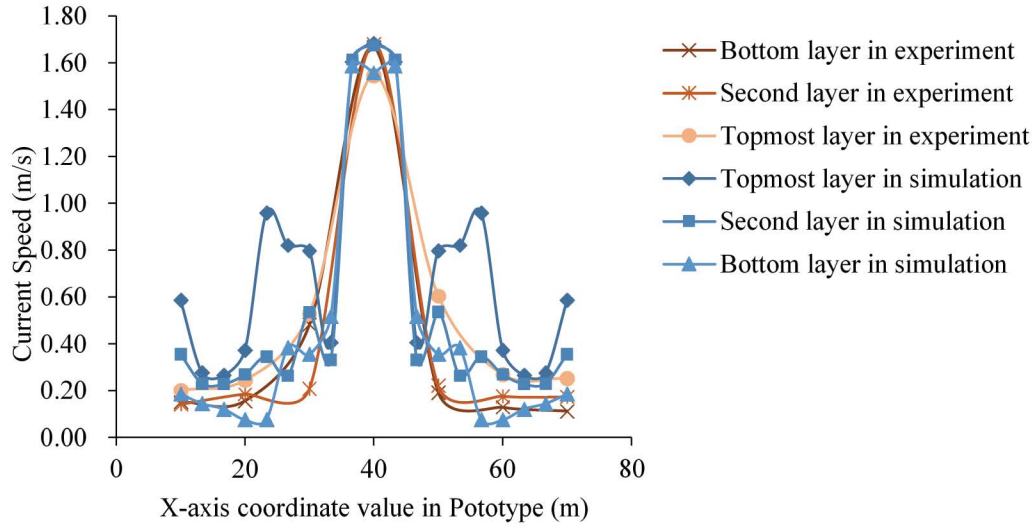

Fig. 24. Comparative chart of 7-7 sectional velocity of numerical simulation with experimental results under flood condition of once in 50 y.

simulation on the 7-7 section is relatively different from experimental data. This is mainly due to the simplified free water surface in the numerical simulation process causing the surface narrowing. The water surface narrowing when the dam is overflowed will cause the instability of velocity, and the velocity in this kind of position is much bigger. In the experiment, the influence of surface narrowing is relatively smaller, because the geometry scale in the experiment is 1:20. As such, the flow velocity of the topmost layer obtained by numerical simulation has greater change and the bigger flow rate.

In Fig. 25 the main difference occurs in the flow velocities distribution of the second layer, and the situations of the 7-7 section and 8-8 section are similar. There is an obvious difference between simulation and experiment in the 11-11 section of Fig. 26, the experimental data are smaller than the results of numerical simulation. And there is an obvious deviation between these two curves. It maybe that the downstream segment is too short, causing the numerical model does not reach the equilibrium point. In addition, the pumping device to pump water at the downstream gate also affects the direction of water flow.

The above is the comparison of the numerical simulation and model experiment in each section along the x-axis direction, and the following is to discuss the velocity change along the y-axis. The analysis is conducted by selecting the topmost layer, second layer and bottom layer on the middle lines of each section.

Fig. 27 is the comparative diagram of the flow velocity distribution of numerical simulation along the water flow direction. The main difference occurs at the gate pier contraction segment and downstream segment, and the blocking

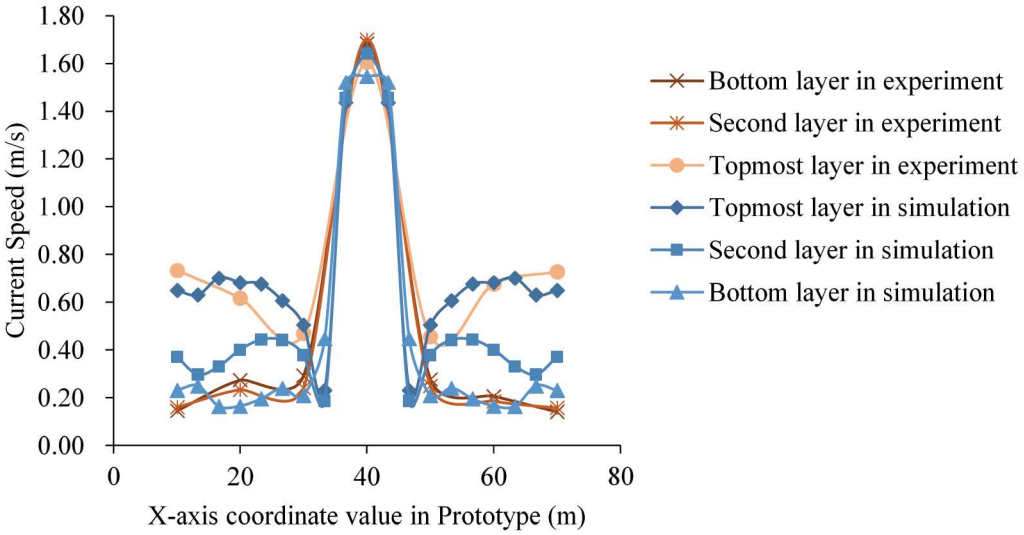

Fig. 25. Comparative chart of 8-8 section velocity of numerical simulation with experimental results under flood condition of once in 50 y.

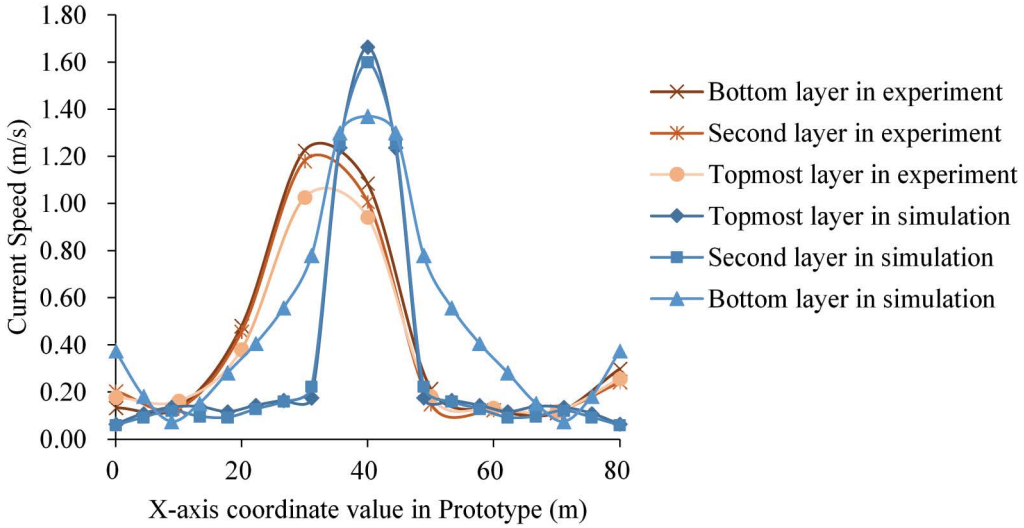

Fig. 26. Comparative chart of 11-11 section velocity of numerical simulation with experimental results under flood condition of once in 50 y.

effect of the gate pier seems to be bigger than expected. The gate pier's effect on water flow can be explained as:

It can be seen in Fig. 19 that there is a dramatic velocity change along the *x*-direction in the 7-7 section located at a distance of 3.088 m from the bottom in comparison with other water depths (0.618, 1.236, 1.854 and 2.470 m), and the velocities on both sides of the other layers are smaller. Through the analysis, the reason for flow velocity changes of the topmost measuring points is that the sectional water level is much higher than the overflow dam, forming a larger water level drop to form a large flow velocity. Then there is a hydraulic drop at the downstream gate because we have set up a steep slope between the downstream segment and stilling basin. Hydraulic drop is a type of local phenomenon found in open channel flow. It is a rapid change in the depth of flow from a high stage to a low stage that results in a steep depression in the water surface. The steep slope and stilling basin are mainly used to alleviate the high water momentum of a hydraulic drop. As such, the steep slope could decrease the water flow rate, and this is another reason why the flow velocity obtained from the experiment is smaller.

The common feature of each working condition is that the upper flow state is more complicated than the bottom flow state, and the flow velocity changes more severely according to Table 2. Then the velocity of the water flow of once in 20 y is the smallest. For the once in 50 y, the topmost layer water flow is obviously more torrent than the bottom water flow, resulting in a larger vortex. The water flow of once in 100 y is the most urgent and its vortex is the most.

Figs. 28–33 are the flow regimes of the bottom and surface of the physical model under conditions of once in

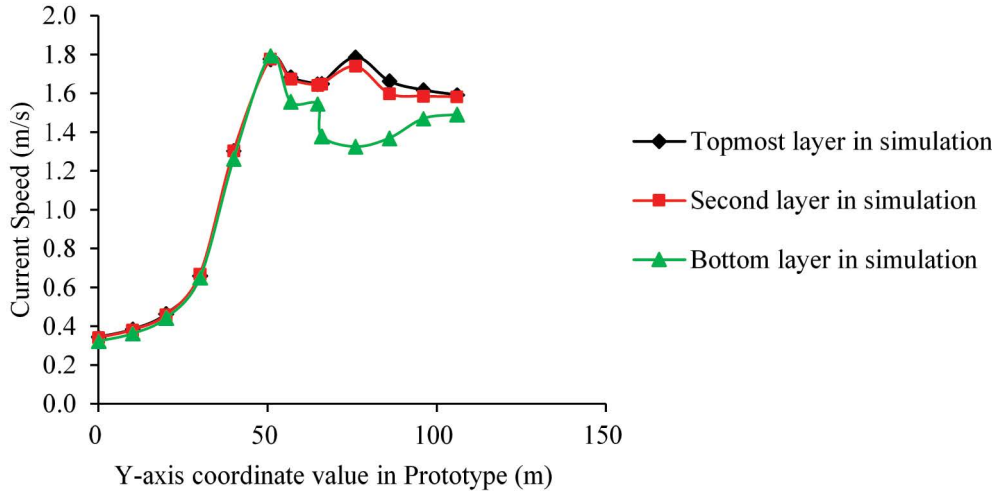

Fig. 27. Comparative chart of flow velocity distribution along the flow direction under flood condition of once in 50 y.

Table 2
Flow velocity distribution of bottom and topmost layers under three flood conditions

Test sections	Flow velocities of once in 20 y (m/s)		Flow velocities of once in 50 y (m/s)		Flow velocities of once in 100 y (m/s)	
	Bottom layer	Topmost layer	Bottom layer	Topmost layer	Bottom layer	Topmost layer
1	0.231	0.279	0.257	0.304	0.256	0.307
2	0.245	0.288	0.272	0.319	0.264	0.325
3	0.258	0.291	0.304	0.341	0.274	0.351
4	0.324	0.358	0.379	0.434	0.303	0.340
5	0.479	0.670	0.677	0.698	0.667	0.667
6	0.512	0.563	0.800	0.828	0.771	0.801
7	0.535	0.541	0.413	0.518	0.821	0.731
8	0.511	0.521	0.431	0.730	0.733	0.751
9	0.482	0.518	0.532	0.614	0.621	0.611
10	0.470	0.434	0.480	0.536	0.580	0.561
11	0.422	0.349	0.423	0.458	0.483	0.424
12	0.473	0.383	0.402	0.384	0.535	0.428
13	0.485	0.448	0.419	0.379	0.337	0.411

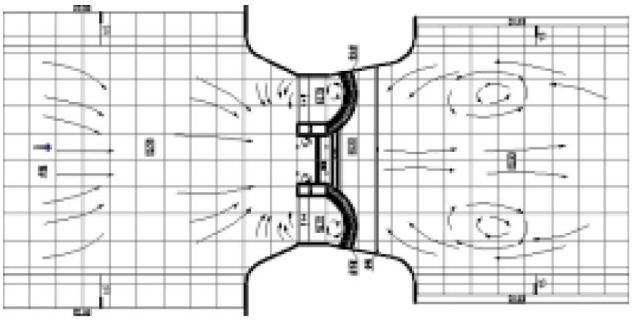

Fig. 28. Bottom flow regime of once in 20 y.

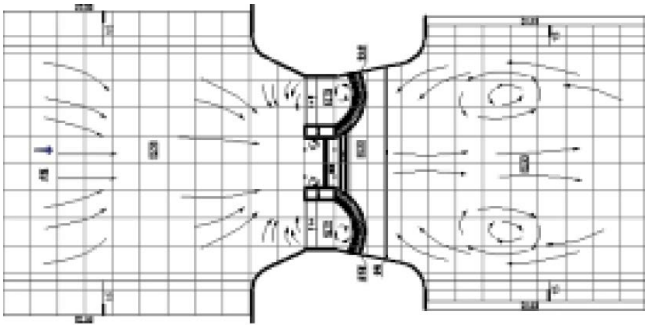

Fig. 29. Top flow regime of once in 20 y.

20 y, once in 50 y, and once in 100 y. Water flows from the upstream after entering through the gate upstream segment is relatively stable, and when the flow approaches the hoist chamber, the flow cross-section size changes, causing the water flow is gradually moving toward the central axis. A small part of the water flow moves to both sides of the dam and forms a whirlpool with micro rotational speed. Two tiny swirling flows are formed at each side of

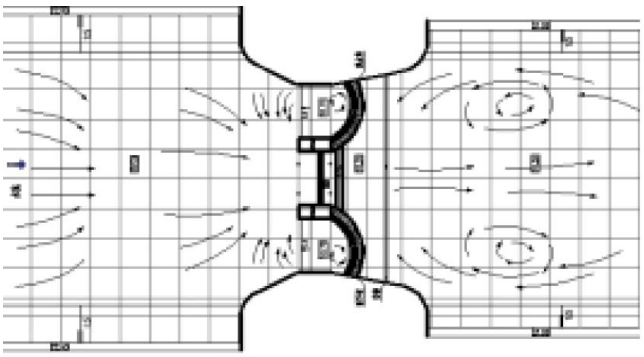

Fig. 30. Bottom flow regime of once in 50 y.

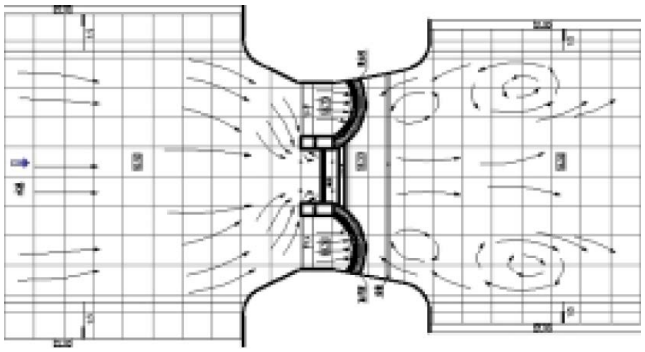

Fig. 31. Top flow regime of once in 50 y.

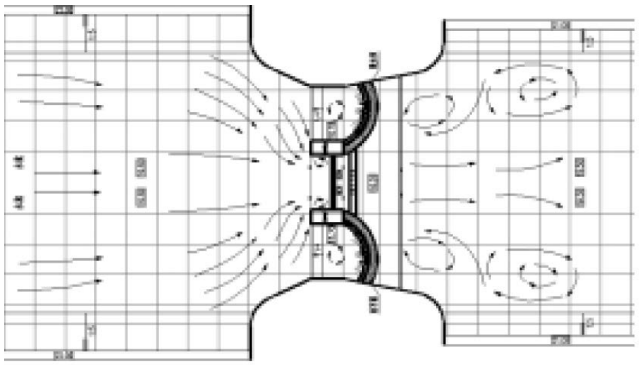

Fig. 32. Bottom flow regime of once in 100 y.

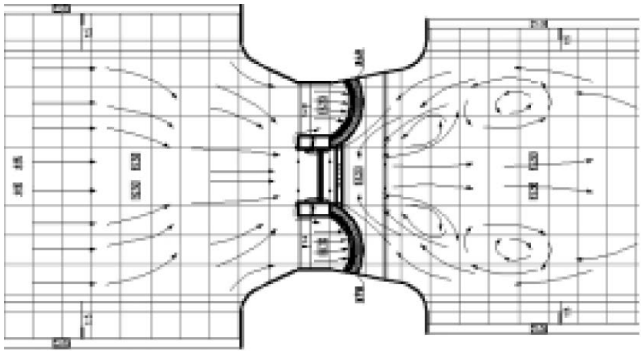

Fig. 33. Top flow regime of once in 100 y.

the opening and closing chamber. After going through the chamber section, most of the water streams flow downstream, and there is a small part of the water streams affected by the increase of overflow section, forming raceways on either side of the river.

6. Conclusions

Through numerical simulation analysis and physical model experiment, this paper completed the measurement and analysis of the flow velocity and flow pattern on the bottom shaft driving flap gate project under three flood conditions to study the turbulent flow next to the gate. This study of the bottom shaft driving flap gate water flow pattern can not only verify the rationality of this type of gate, but can also offer a reference for the application study of similar projects.

The bottom shaft driving flap gate numerical simulation calculation used CFD software with the aid of the mapping software AutoCAD to complete the geometric modeling. Then the geometric model was imported into CFX ANSYS software with the ICEM CFD ANSYS preprocessor. By using the ICEM CFD ANSYS's strong grid partition function, the model was divided into grids by using the tetrahedral type of structured grid. Finally, the flow line, flow chart, and flow velocity vector diagrams of the model were obtained by solving the CFX solution. At the same time, the data at the same position of the test section was extracted, and the flow velocity curves of each typical section were obtained. On the basis of flow velocity distribution charts, it was concluded that the water flow situation under the flood condition of once every 20 y is relatively gentle, the water flow situation of flood condition occurring once every 50 y is very similar to that of flood condition occurring once every 100 y, and the whirlpools of these three flood conditions mainly occur in the downstream central location. This is because the water flows through the overflow dam (once every 50 y and once every 100 y) will form a water level difference, causing the downstream water level to be relatively disordered. According to the flow velocity cloud pictures of the three flood conditions, the largest flow velocity mainly occurs in the vicinity of the narrowing segment of the pier section.

Then the numerical simulation results were compared with the experimental results. Overall, the results of the simulation and experiment were consistent, and the difference mainly occurred in the downstream section. That is because the water in the model experiment was controlled by a circulating water supply system, the downstream water flow was affected by pumping force causing some deviation. At the gate pier contraction segment and downstream segment, the flow velocity obtained by simulation is generally higher than the flow velocity obtained from the experiment. The major reasons are: (1) The blocking effect of gate pier is bigger in practical application. (2) There are steep slopes and stilling basins at the downstream gate to alleviate the high water momentum.

Acknowledgments

This work was supported by the Major Science and Technology Project of the Xinjiang Production and

Construction Corps (No. 2018AA003), the Major science and technology project of Xinjiang Uygur autonomous region (Grant No.2016A03008-02), the Project funded by the China Postdoctoral Science Foundation (Grant No. 2019M663121).

References

[1] V.T. Nguyen, 3D numerical simulation of free surface flows over hydraulic structures in natural channels and rivers, J. Appl. Math. Model.l, 39 (2015) 6285–6306.
[2] N.R.B. Olsens, H.M. Kjellesvig, Three-dimensional numerical flow modelling for estimation of spillway capacity, J. Hydraul. Res., 36 (1998) 775–784.
[3] Y. Guo, X. Wen, C. Wu, D. Fang, Numerical modelling of spillway flow with free drop and initially unknown discharge, J. Hydraul. Res., 36 (1998) 785–801.
[4] C.S. Song, F. Zhou, Simulation of free surface flow over spillway, J. Hydraul. Res., 125 (1999) 959–967.
[5] B.M. Savage, M.C. Johnson, Flow over ogee spillway: physical and numerical model case study, J. Hydraul. Res., 127 (2001) 640–648.
[6] C. Biscarini, S.D. Francesco, P. Manciola, CFD modelling approach for dam break flow studies, Hydrol. Earth Syst. Sci., 14 (2010) 705–718.
[7] V.T. Nguyen, F. Nestman, Applications of CFD in hydraulics and river engineering, Int. J. Comput. Fluid Dyn., 18 (2004) 165–174.
[8] S. Ghosal, P. Moin, The basic equations for large eddy simulation of turbulent flows in complex geometry, J. Comput. Phys., 118 (1995) 24–37.
[9] T.S. Lund, X. Wu, K.D. Squires, Generation of turbulent inflow data for spatially-developing boundary layer simulations, J. Comput. Phys., 140 (1998) 233–258.
[10] M. Klein, A. Sadiki, J. Janicka, A digital filter based generation of inflow data for spatially developing direct numerical or large eddy simulations, J. Comput. Phys., 186 (2003) 652–665.
[11] A. Ferrante, S.E. Elgobashi, A robust method for generating inflow conditions for direct simulations of spatially-developing turbulent boundary layer, J. Comput. Phys., 198 (2004) 372–387.
[12] I.S. Kholopov, M.I. Balzannikov, A.O. Lukin, A.V. Solovjev, On spatial lattice metal structures use in roofing of mechanical equipment rooms of hydroelectric power stations, Vestnik MGSU, 11 (2013) 34–41.
[13] V.Y. Alpatov, A.A. Lukin, The method of mirror functions in optimal design of pre-stressed spatial structures, Procedia Eng., 111 (2015) 20–29.
[14] F.H. Harlow, J.E. Welch, Numerical calculation of time-dependent viscous flow of fluid with free surface, Phys. Fluids, 8 (1965) 2182–2189.
[15] F.H. Harlow, J.F. Welch, Numerical study of large-amplitude free-surface motions, Phys. Fluids, 9 (1966) 842–851.
[16] C.W. Hirt, B.D. Nichols, Volume of fluid (VOF) method for the dynamics of free boundaries, J. Comput. Phys., 39 (1981) 201–225.
[17] R. Fedkiw, T. Aslam, A non-oscillatory eulerian approach to interfaces in multimaterial flow (the ghost fluid method), J. Comput. Phys., 152 (1999) 457–492.